Feasibility of Deep Convolution Neural Network-Based Automatic Time Activity Curve Fitting Method for Non-Invasive Cerebral Blood Flow Quantification

Rieko NAGAOKA[1)], Kosuke YAMASHITA[1)], Naohiro YABUSA[1)], Ryosuke KAMEZAKI[2)], Ryuji IKEDA[2)], Shinya SHIRAISHI[3)], Yoshikazu UCHIYAMA[4)], and Shigeki ITO[5)*]

[1)] Graduate School of Health Sciences, Kumamoto University
[2)] Department of Central Radiology Kumamoto University
[3)] Department of Diagnostic Radiology, Faculty of Life Sciences, Kumamoto University
[4)] Department of Information and Communication Technology, Faculty of Engineering, University of Miyazaki
[5)] Department of Medical Radiation Sciences, Faculty of Life Sciences, Kumamoto University

Received Dec. 18, 2023; accepted Jan. 10, 2024

In this study, we aimed to develop a deep convolutional neural network (DCNN)-based automatic time–activity curve (TAC) fitting method for input function determination. This will be achieved through a comparison between the DCNN method, manual method, and mathematical fitting methods using the expectation maximization algorithm (EM-method) to uncover the potential of the DCNN approach.

A U-Net architecture based on convolutional neural networks was used to determine the TAC fittings. The area under the curve (AUC) values of the TAC by the EM and DCNN methods were compared to those obtained using the manual method.

The AUC values for the EM-manual method exhibited similarity within an error range of approximately ±20%. Conversely, the error range for DCNN-manual method was approximately ±10%, signifying a reduction in the error range to approximately 1/2.

Our findings indicate that the DCNN method provides accuracy equivalent to those of manual methods and even slightly superior to that of the EM method.

Key Words: ^{123}I-IMP; ^{99m}Tc-ECD; area under the curve; deep neural network; rCBF quantification

[doi:10.12950/rsm.231218]

Introduction

Non-invasive (pain free) methods for quantifying cerebral blood flow offer advantages such as minimal discomfort and procedural simplicity in nuclear medicine, as they enable the acquisition of input functions from radioactive concentrations in arterial blood without the need for arterial blood sampling[1–3)]. In recent years, a non-invasive quantification method using N-isopropyl-p-[^{123}I] iodoamphetamine (^{123}I-IMP), known as the Simple Non-Invasive Microsphere (SIMS) method (^{123}I-IMP SIMS), has been developed[4–6)]. Additionally, for the ^{99m}Tc-ethyl cysteinate dimer (^{99m}Tc-ECD), an Improved Brain Uptake Ratio (IBUR) method (^{99m}Tc-ECD IBUR) has been developed based on aortic hemodynamics[7–9)]. In these methods, estimating the administered dose involves setting a region of interest (ROI) in the pulmonary artery (PA) and ascending aorta (AAo) during ^{123}I-IMP and ^{99m}Tc-ECD chest radio-isotope (RI)-angiography and determining the radioactive concentration in arterial blood from the integral value of the obtained time-activity curves (TACs)[4–9)]. However, due to manual curve analysis, these methods heavily rely on the operator's skills and are less

* Department of Medical Radiation Sciences, Faculty of Life Sciences, Kumamoto University
E-mail: shigekii@kumamoto-u.ac.jp
Tel: +81-96-373-5482

reproducible and accurate when compared to invasive quantification methods[3]. Consequently, there is a need to enhance the reproducibility and measurement accuracy of non-invasive quantification methods.

To address these issues, automatic TAC fitting is the most suitable approach, and for automation, both mathematical and deep learning approaches are being considered[10–12]. In mathematical approaches, optimization algorithms, such as the least squares method, are used to find the best fit of functions, like the Gamma function, to data points. This approach is effective when the data is relatively simple and easily modelled.

Among Deep Convolutional Neural Networks (DCNNs), U-net excels in image segmentation and is widely applied in the field of medical imaging[13–17]. Particularly, the use of an autoencoder to perform noise reduction in waveforms based on features learned from normal examples could lead to further improvements in the accuracy of TAC fitting. Furthermore, these automations achieve high reproducibility and accuracy independent of operator skills. Once automatic TAC fitting is completed, there will be no need for confirmatory tasks, leading to improved operational efficiency and a significant reduction in analysis time. At present, it is not clear which approach, mathematical or DCNN, is effective for the ^{123}I-IMP SIMS and ^{99m}Tc-ECD IBUR methods. Therefore, it is necessary to clarify the accuracy of both approaches.

The objective of this research was to develop a DCNN-based automatic TAC fitting method for input function determination in non-invasive cerebral blood flow quantification methods, specifically the ^{123}I-IMP SIMS method and the ^{99m}Tc-ECD IBUR method, within the field of nuclear medicine. This was achieved by comparing the DCNN method, manual methods, and mathematical fitting methods to uncover the potential of the DCNN approach.

Methods

Ethics statements

This research received approval from the Ethics Committee of Medicine at Kumamoto University for Human Studies, with Protocol Number: Advanced 1451, dated September 29, 2022. Prior to commencing the study, written informed consent was obtained from all participating patients. Furthermore, all image data underwent anonymization procedures, and the study was conducted in strict adherence to the ethical principles outlined in the Declaration of Helsinki, as well as the specific regulations of the ethics committees of each participating institution.

This study was a retrospective, comparative, observational investigation that aimed to develop an automated TAC fitting program using deep neural networks. This study is reported according to the Strengthening the Reporting of Observational Studies in Epidemiology guidelines.

Participants

The study included 84 patients (male: 37, female: 47, mean age: 76.5 years) who underwent ^{123}I-IMP RI-angiography and microsphere imaging at the same time and 94 patients (male: 69, female: 25, mean age: 69.7 years) who underwent ^{99m}Tc-ECD single photon emission computed tomography (SPECT) and RI angiography between February 2012 and September 2017 at Kumamoto University Hospital. None of the patients had pulmonary disease.

^{123}I-IMP chest RI-angiography was performed using a SPECT device (Millennium VG, GE, USA). Imaging was performed at 1 fps for 60 s after the ^{123}I-IMP bolus injection. The matrix size was 128×128 pixels, and the pixel size was 2.2 mm. Collimators were equipped with low energy and high resolution (LEHR). The energy window was set to 159 keV $\pm$ 10%.

^{99m}Tc-ECD chest RI angiography was performed using a SPECT device (E-cam, SIEMENS, Germany). Imaging was performed at 1 fps for 100 s from the start of the ^{99m}Tc-ECD bolus injection. The matrix size was 128×128 pixels, and the pixel size was 2.2 mm/pixel. A LEHR collimator was used. The energy window was set to 140 keV $\pm$ 10%. The Daemon Research Image Processor (PDRadiopharma Inc., Japan) and Image J (National Institute of Health, USA)[18,19] were used for image processing.

DCNN condition for TAC fitting

Figure 1 shows the structure of a DCNN (U-net)[16,17]. We applied the leaky rectified linear unit (Leaky ReLU) activation function and batch normalization to all convolutional layers, except for the last convolutional layer in the U-net, with depths of 5 and 13 convolutional layers. Immediately after the last convolutional layer, the squared error was applied to the output layer. The optimization functions for the U-net training were adaptive moment estimation (Adam), Alpha = 0.001, Beta1 = 0.9, Beta2 = 0.999, and Epsilon = 1E-8, and the number of iterations was 1000. For the learning and validation of the U-net, all samples were randomly divided into six groups, and all cases were evaluated using six-fold cross-

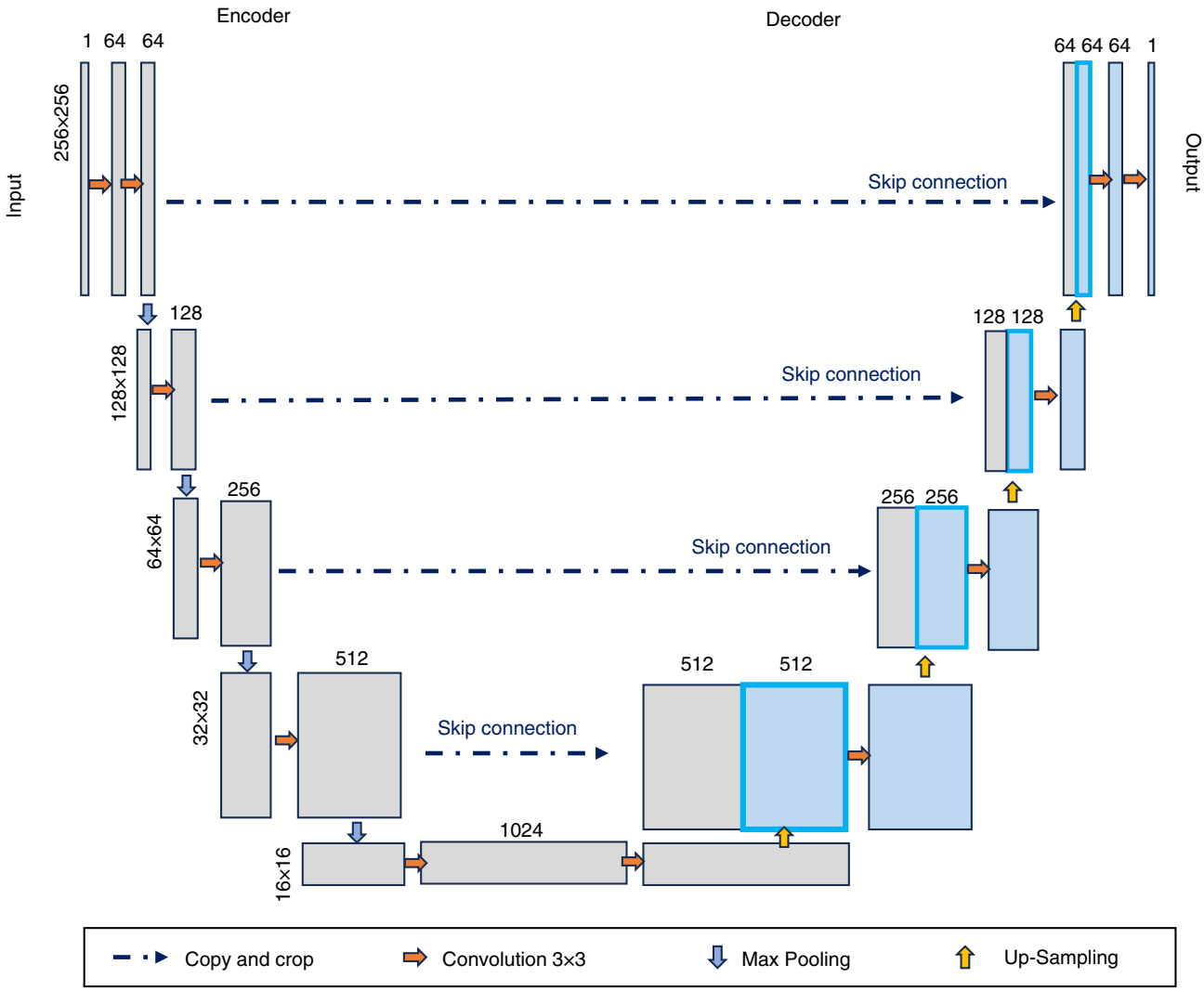

Fig. 1.Structure of a DCNN (U-net)

validation. The operating environment used was Microsoft Windows 11 Pro, the CPU was an Intel Xeon E5-2623 v3, and the GPU was an NVIDIA Quadro RTX6000. The program was developed using Sony Neural Network Console.

Manual fitting (manual)

Manual fitting involves dividing the TAC into two segments, before and after the peak, as the rising and falling portions of the TAC curve can vary depending on the patient and the speed of drug administration. Each of these segments was then fitted individually using Gaussian functions. Figure 2 illustrates the procedure of manual curve fitting conducted to show the cumulative range of TACs and the AUC for both the ^{123}I-IMP SIMS method and the ^{99m}Tc-ECD IBUR method. In the initial segment, the cursor was positioned approximately two-thirds of the way from the starting point to the peak in order to faithfully replicate the vicinity of the peak. From the peak, the cursor was set to approximately one-third of the way to the endpoint for similar reason. After curve fitting using two Gaussian functions, the AUC was calculated. The fitting parameters for each segment were determined by 2 nuclear medicine specialists and 3 researchers with expertise in nuclear medicine, using the same techniques as the development of the ^{123}I-IMP SIMS and ^{99m}Tc-ECD IBUR methods[4,7]. The TAC data were used as training data and for control purposes. The AUC values (counts/cm^2) were calculated as the average of five sets of TAC data.

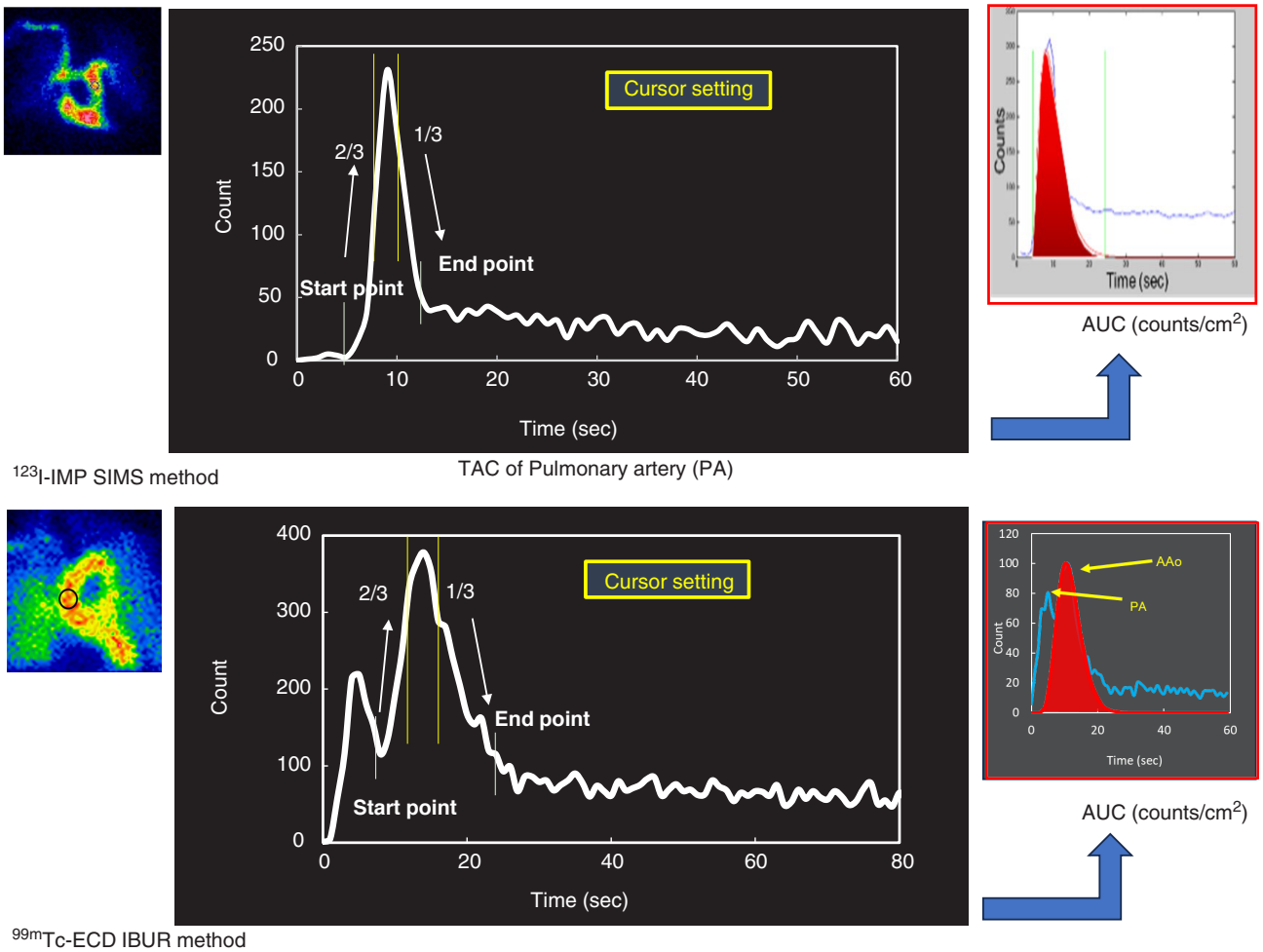

Fig. 2. Procedure of manual curve fitting

EM-algorithm fitting

The gamma distribution is a type of continuous probability distribution characterized by two parameters[20]. The probability density function of a one-variable gamma distribution is defined by Equation (1.1).

$$f(x|\alpha,\beta)=\frac{x^{\alpha-1}}{\Gamma(\alpha)\beta^{\alpha}}e^{(-x/\beta)} \qquad (1.1)$$

Furthermore, the mean (expected value) E(X) and variance V(X) of the gamma distribution can be expressed using equations (1.2) and (1.3).

$$\mathrm{E(X)}=\alpha\beta \qquad (1.2)$$

$$\mathrm{V(X)}=\alpha\beta^{2} \qquad (1.3)$$

Here, α represents the shape parameter, β represents the scale parameter, and $\Gamma(\alpha)$ denotes the gamma function. Both α and β are positive values. The gamma distribution can accommodate various shapes depending on the choice of α and β[21–24].

Parameters of the gamma distribution

The properties and shape of the gamma distribution are determined by two parameters, α and β, as described in Equation (1.1). Therefore, by determining the parameters of each gamma distribution from the TACs with gamma distributions, it is possible to estimate a single gamma distribution TAC that matches the desired peak.

As the mean of the gamma distribution, as shown in Equation (1.2), is the product of the two parameters, we used this property to determine the initial values of the parameters.

Assuming the mean of the gamma distribution to be the peak, setting $\beta = 1$ allows us to set α to the time detected by the peak detection program.

In the case of the IBUR method, which employs a mixed gamma distribution with two gamma distributions, the initial values of the parameters can be expressed using Equation (1.4).

$$\alpha_1 = peak1, \quad \alpha_2 = peak2, \quad \beta_1 = 1, \quad \beta_2 = 1 \qquad (1.4)$$

Furthermore, let ε represent the fraction that each gamma distribution occupies in the mixture gamma distribution. Since the total of ε should sum to 1, the initial values for the mixture ratios in the IBUR method can be expressed using Equation (1.5).

$$\varepsilon_1 = 0.5, \quad \varepsilon_2 = 0.5, \quad \varepsilon_{total} = 1 \qquad (1.5)$$

Parameter estimation using the EM algorithm

Parameter calculation was performed using the EM algorithm[18]. The EM algorithm is executed by iterating through two processes: the E-step and the M-step[22]. Figure 3 illustrates an overview of the EM algorithm implemented in this program.

Initially, we prepared input data and parameters given initial values, and then executed the EM algorithm using these data. In the E-step, we calculated the probability that the i-th data point, denoted as xi, belongs to the k-th gamma distribution (membership probability) $z_{ik}^{(t)}$ using Equation (1.6).

$$z_{ik}^{(t)} = \frac{f(x_i|\alpha_k^{(t)}, \beta_k^{(t)})}{\Sigma_{l=1}^{k} \varepsilon_l^{(t)} f(x_i|\alpha_l^{(t)}, \beta_l^{(t)})} \qquad (1.6)$$

In this context, $f(x|\alpha, \beta)$ represents the formula for the gamma distribution, and the subscript 't' denotes the iteration count.

After calculating the membership probabilities in the E-step, we used these probabilities to update the parameters for each gamma distribution in the M-step. The parameters determined when α converged were then considered as the parameters for the gamma distribution.

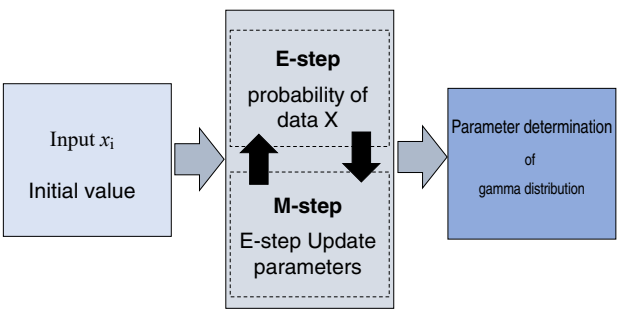

Fig. 3. EM Algorithm

DCNN fitting

Figure 4 illustrates an overview of the training process for the TAC automatic fitting program using U-net as an autoencoder.

One-peak original chest RI-angiography and manual fitted TACs obtained from 50 patients (male:21, female: 29, mean age: 73.9 years) images by setting the ^{123}I-IMP PA as the ROI and two-peak original and manual fitted TACs from 44 patients' (male: 20, female: 24, mean age: 60.3 years) images by setting the ^{99m}Tc-ECD AAo as the ROI were used as the training and validation datasets, respectively.

The image format required for DCNN processing is the Portable Network Graphics (PNG) format. Therefore, TACs were converted to the PNG format using our original program developed in the Python programming language. All images were processed as detailed above and, then, prepared as 256×256 matrices. Additionally, by performing expansion of the curve along the x-axis and y-axis, the number of images was augmented 32-fold, and the learning data set was prepared. For the final image, the PNG image obtained using DCNN was reformatted into a TAC using the original image pixel counts.

Evaluation

The final test dataset of one-peak TACs for the ^{123}I-IMP SIMS method comprised data from 34 (male: 15, female: 19, mean age: 60.3 years) out of 84 patients. For the two-peak TACs for the ^{99m}Tc-ECD IBUR method, the final test dataset included data from 50 (male: 29, female: 21, mean age: 61.3 years) out of 94 patients who underwent ^{99m}Tc-ECD RI-angiography at Kumamoto University Hospital.

To assess the utility of DCNN fitting, we compared the obtained AUC values in counts/cm^2 between the manual method (used as control data) and the EM and DCNN methods, thereby elucidating the advantages of DCNN.

Statistical analysis

In this study, we investigated the relationship between AUC values obtained using three different fitting methods: manual, EM, and DCNN. We used correlation analysis to assess the degree of association between these AUC values, and the Pearson correlation coefficient (r) was calculated. We utilized MedCalc Statistical Software version 20.115 (Med Calc.

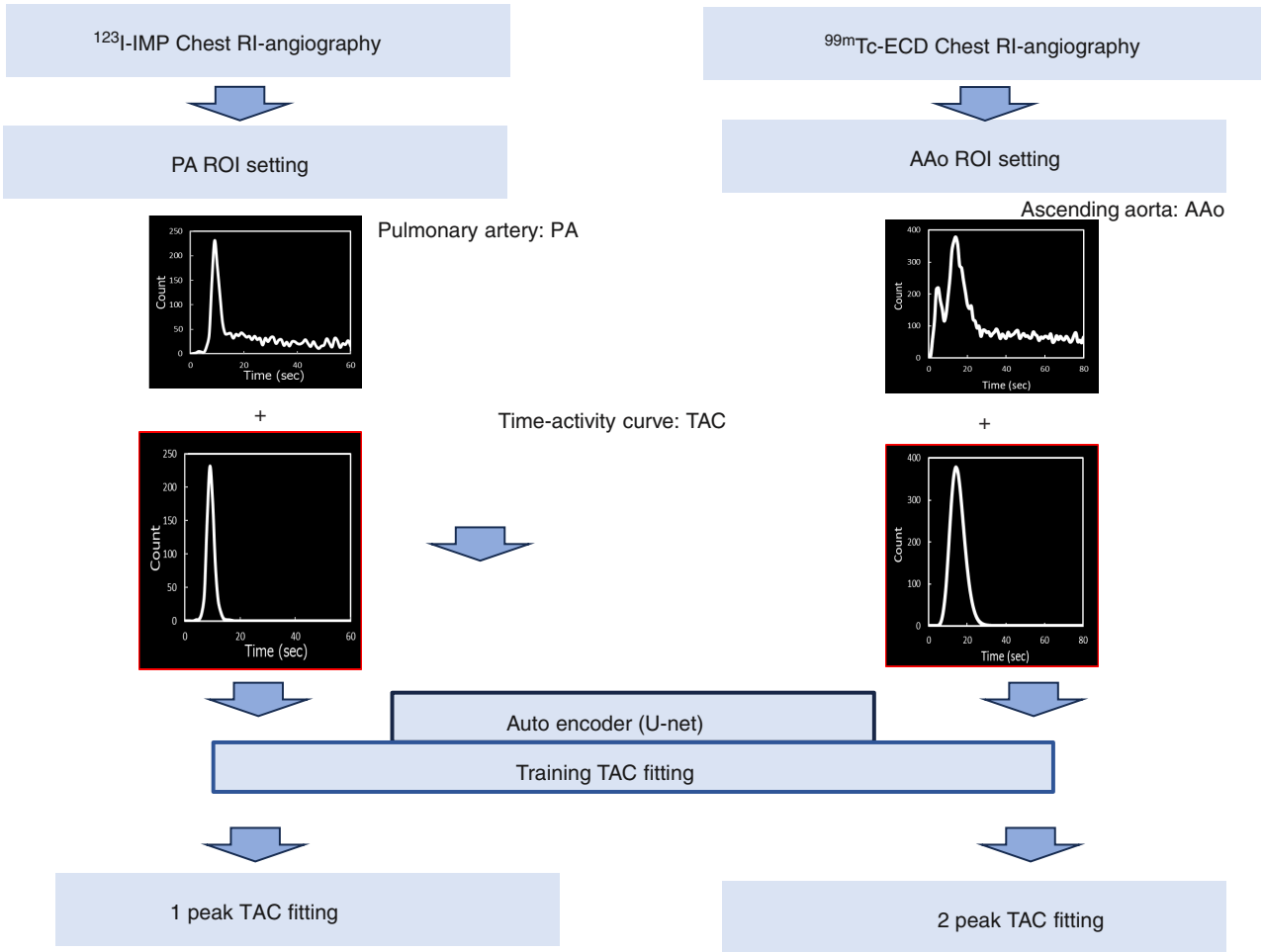

Fig. 4. Training process for the TAC automatic fitting program using U-net as an autoencoder.

Software Ltd., Ostend, Belgium) for the statistical analysis. Statistical significance was set at $p<0.001$. To further evaluate the agreement between the AUC values obtained by the manual, EM, and DCNN fitting methods, we employed the Bland–Altman analysis. This method allows us to assess the level of concordance between the measurements of these variables. The Bland–Altman plot displays the differences between measurements on the y-axis and the averages of measurements on the x-axis. When the plotting data points cluster closely around zero, it indicates good agreement with minimal systematic bias.

Results

Figures 5a and 5b show the overlaid plots of the monomodal TAC and bimodal TAC, respectively, obtained using the DCNN method and the original TAC obtained by the manual method. Visually, a good match is observed. Similar TAC fitting results as in Figures 5a and 5b were obtained for other cases as well.

Figure 6a depicts the relationship between AUC values for perfusion assessment using the ^{123}I-IMP SIMS method obtained manually and through EM. The relationship between the EM AUC (y) and manual AUC (x) is described by $y = 0.961x + 2.822$, with a correlation coefficient of 0.97. In the Bland–Altman plot, the mean difference is 2.0%, and the 1.96 standard deviation (SD) is approximately ±22%, indicating a good agreement between the two methods.

Figure 6b illustrates the relationship between AUC values obtained manually and that obtained through DCNN. The relationship between the DCNN AUC (y) and manual AUC (x) is expressed as $y = 1.004x - 2.043$, with a higher correlation coefficient (0.99) compared to that of the previous case. In the

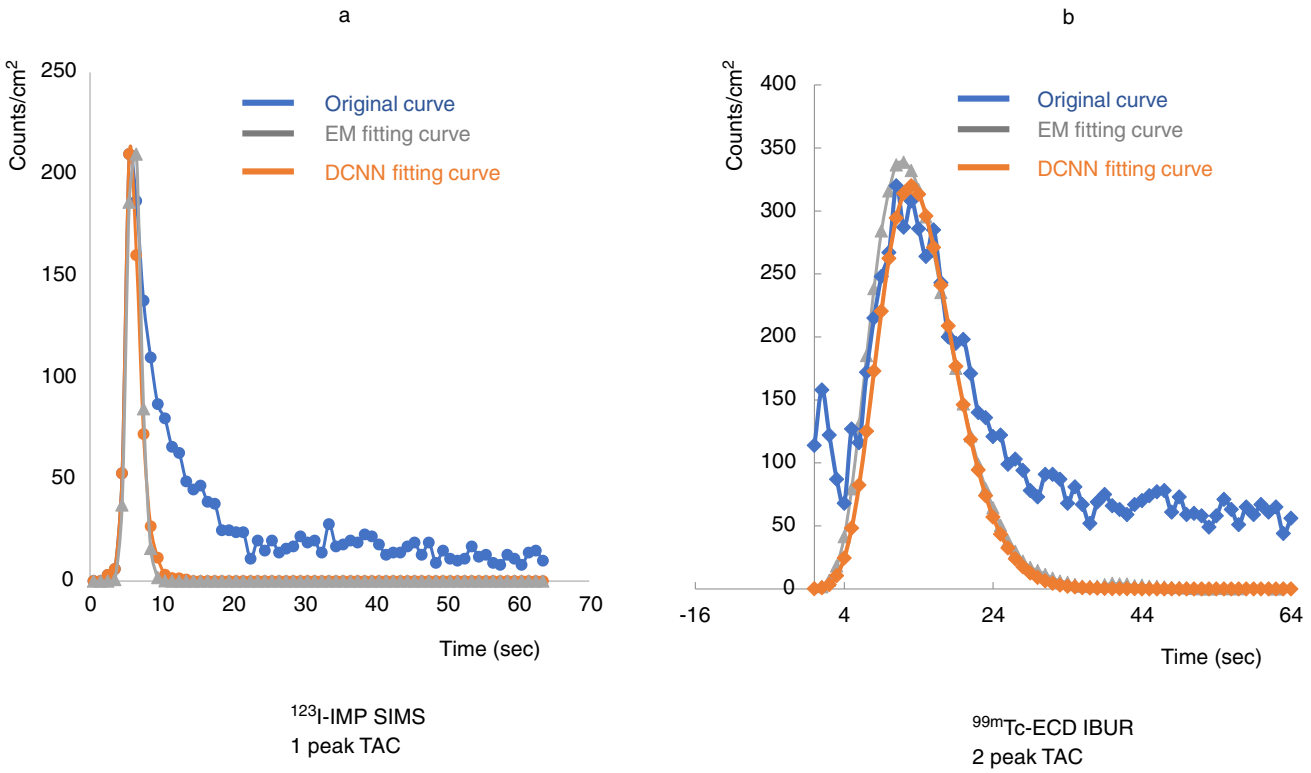

Fig. 5. TAC fitting. a: ^{123}I-IMP SIMS 1peak TAC, b: ^{99m}Tc-ECD IBUR 2 peak TAC.

Bland-Altman plot, the mean difference is 1.1%, and the 1.96 SD is approximately ±15%, showing that the DCNN method exhibits even better agreement with the manual method. No systematic errors were observed in either case.

Figure 7a illustrates the relationship between AUC values obtained by the manual and EM methods for the AAo using the ^{99m}Tc-ECD IBUR method. The relationship between the EM AUC (y) and manual AUC (x) is described by $y = 0.995x + 7.023$, with a correlation coefficient of 0.93. In the Bland–Altman plot, the mean difference is −1.9%, and the 1.96 SD is approximately ±22%, indicating a good agreement between the two methods.

Figure 7b shows the relationship between AUC values obtained manually and those obtained through DCNN. The relationship between the DCNN AUC (y) and manual AUC (x) is expressed as $y = 1.021x - 2537$, with a higher correlation coefficient (0.99) compared to that of the previous case. In the Bland–Altman plot, the mean difference is −1.0%, and the 1.96 SD is approximately ±8%, showing that the DCNN method exhibits very good agreement with the manual method. No systematic errors were observed in either case.

Discussion

In this study, we developed an automated TAC fitting program using a DCNN to calculate the curve integrals (AUC) derived from TAC analysis. Additionally, to evaluate TAC fitting, we constructed a mathematical approach using the EM algorithm, which is used in clinical practice. By comparing the AUC obtained through the manual, EM, and DCNN methods, we clarified the accuracy of the DCNN method.

Both the one-peak TAC for ^{123}I-IMP SIMS method and the two-peak TAC for ^{99m}Tc-ECD-IBUR method showed good matches with the original TACs obtained by the manual method, as depicted in Figures 6 and 7. According to the Bland–Altman analysis, the AUC values between the EM and manual methods were in agreement within an error range of approximately ±20% for both the ^{123}I-IMP SIMS and ^{99m}Tc-ECD IBUR methods (Figures 6a and 7a). On the contrary, the AUC values between the DCNN and manual methods were in agreement within an error range of ±15% for ^{123}I-IMP SIMS and ±8% for ^{99m}Tc-ECD IBUR methods (Figures 6b and 7b). In other words, the error range for the EM method was approximately twice that of the DCNN method. Therefore, the DCNN method is superior to the EM method.

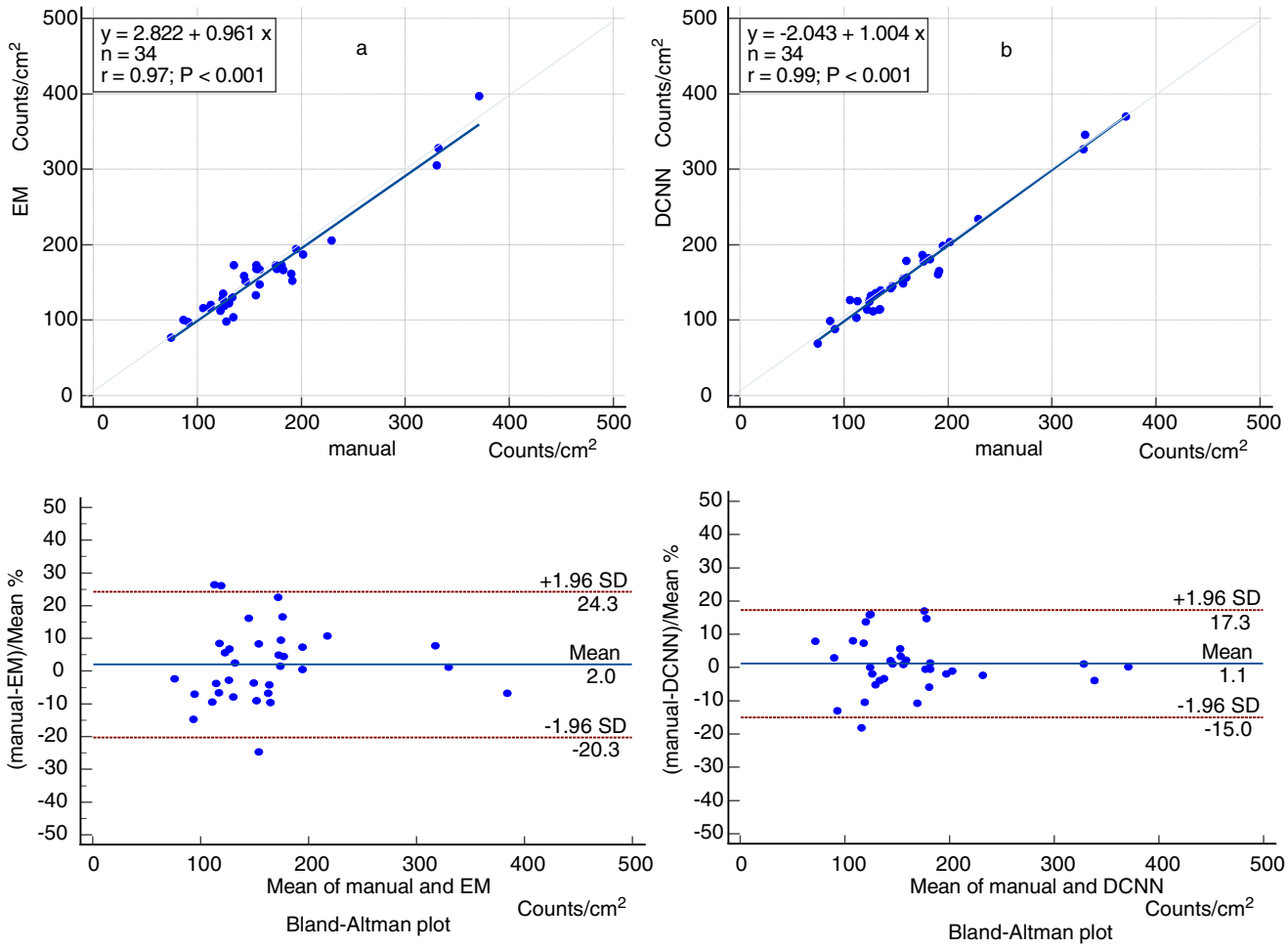

Fig. 6. Relationship between AUC values obtained by the manual and EM methods for the PA using the ^{123}I-IMP SIMS method. a: EM—manual AUC values, b: DCNN—manual AUC values.

In this study, TACs for the ^{123}I-IMP SIMS and ^{99m}Tc-ECD IBUR methods often become complex graphs due to factors such as injection speed and patient-specific characteristics. As a result, a significant amount of time is often spent identifying the optimal functions for TAC analysis[4–7]. In this program, we developed an automated TAC fitting program using a DCNN to calculate the curve integrals (AUC) derived from TAC analysis. Furthermore, we have already developed an automated ROI-setting program based on brain perfusion SPECT image analysis from the SIMS and IBUR methods, allowing fully automated quantitative analysis to be completed within one minute without manual intervention by the operator.

In the manual method, we trained the model using TAC obtained through fitting by experts in non-invasive quantification methods. The DCNN method was designed based on the manual method, faithfully reproducing it. By contrast, the EM method involves a sequential approximation strategy focused on the TAC peak, while the DCNN method offers a more comprehensive fitting strategy believed to be advantageous, especially for capturing the complexities of TACs with multiple peaks. Therefore, the DCNN method, effectively prioritizing clinical input counts over the mathematically accurate EM method, was deemed superior.

By achieving high accuracy in AUC calculations, we can address the challenge of maintaining the precision of input function estimation in non-invasive cerebral blood flow quantification. This advancement is crucial because accurate AUC values are essential for quantifying physiological processes and drug uptake kinetics, directly impacting fields like nuclear medicine and pharmacokinetics[25–29]. Additionally,

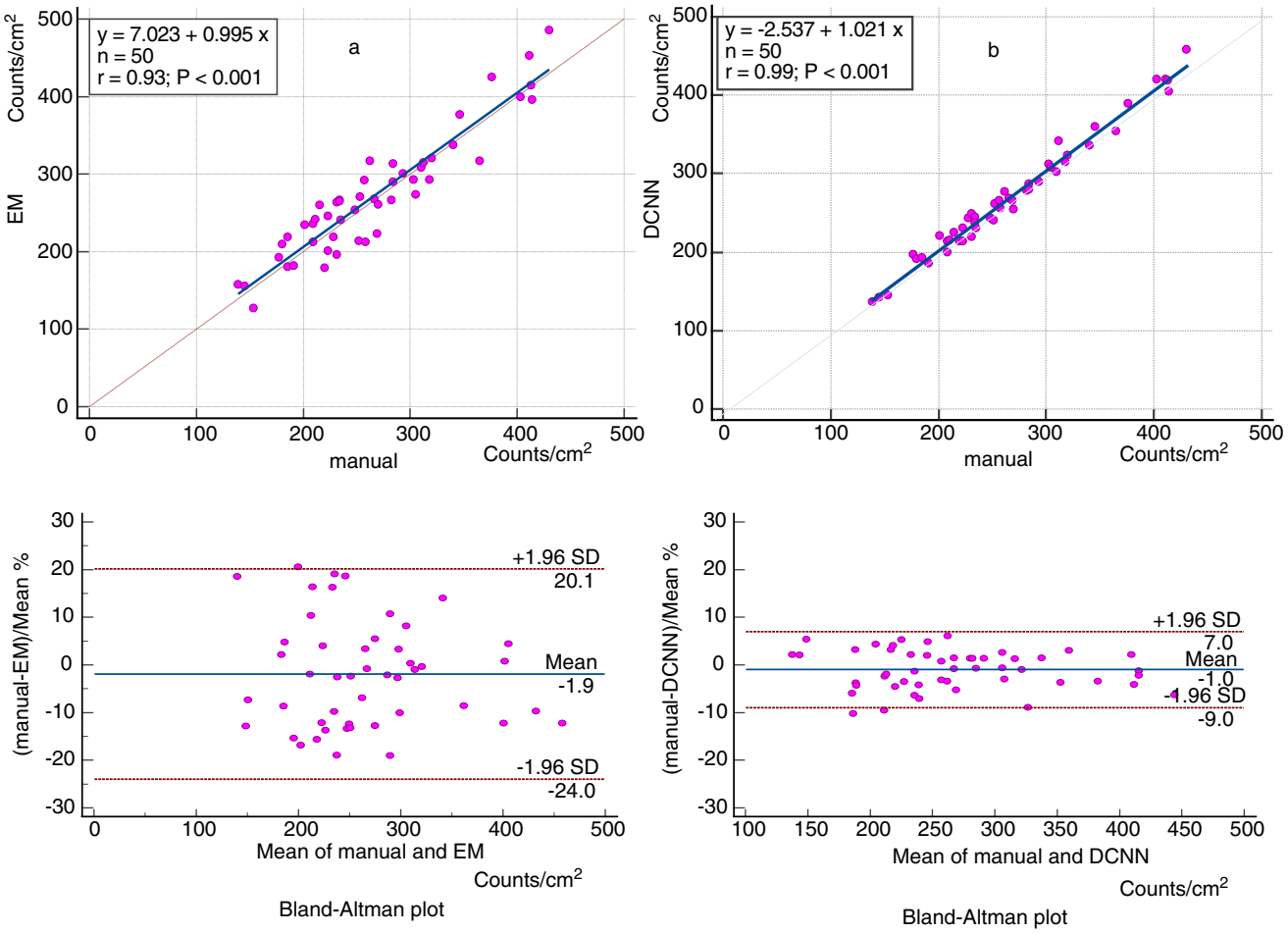

Fig. 7. Relationship between AUC values obtained by the manual and EM methods for the AAo using the ^{99m}Tc-ECD IBUR method. a: EM–manual AUC values, b: DCNN–manual AUC values.

our method suggests the potential for automation in various image analyses and the development of non-invasive quantitative methods across all areas of nuclear medicine examinations in the future.

In this program, we used 34 cases with one-peak TACs and 44 cases with two-peak TACs for training. However, increasing the number of training cases can lead to further improvement in accuracy. Furthermore, while we used cases that were successfully fitted by conventional methods for training, gradually incorporating cases successfully fitted by this program as training examples can lead to the possibility of performing TAC fitting using DCNN alone in the future, which is expected to result in even higher accuracy. Additionally, in this program, we separately trained autoencoders for one- and two-peak TACs and used them for fitting. With improvements in the training methodology, it is conceivable that a program capable of fitting both one- and two-peak TACs can be developed, further simplifying the process.

This study presents results from a single institution. Therefore, it is necessary to conduct validation studies using equipment from several institutions. Regarding the EM method, it was inferior to DCNN, but further improvement in accuracy can be expected through refinements such as revising the approximation formula and adjusting the parameters.

Conclusion

This study aimed to evaluate the effectiveness of the DCNN automatic TAC fitting method for input function determination in non-invasive cerebral blood flow quantification methods, specifically the ^{123}I-IMP SIMS method and the ^{99m}Tc-ECD

IBUR method, within the field of nuclear medicine. Our findings indicate that the DCNN method provides accuracy equivalent to those of manual methods and even slightly superior to that of the EM method. This suggests that the DCNN method has significant potential for clinical application, potentially streamlining and improving the accuracy of non-invasive cerebral blood flow quantification. The clinical significance of these results lies in the potential for enhancing the precision of physiological measurements and drug uptake kinetics in nuclear medicine and pharmacokinetics, ultimately benefiting patient diagnosis and treatment. The ability to automate TAC fitting with high accuracy offers promising opportunities for broader applications within the field of nuclear medicine. For future research, it is essential to validate our findings using different equipment in various facilities to ensure the robustness and generalizability of the DCNN method. Improvements in accuracy can also be explored through modifications to the approximation formula and parameter adjustments in the EM method. This study not only extends our understanding of TAC analysis methods but also paves the way for the clinical application of the DCNN automatic TAC fitting method in various domains. By improving accuracy and streamlining the processes, this research contributes to the advancement of non-invasive quantitative analysis techniques in nuclear medicine and pharmacokinetics, ultimately benefiting patient care and diagnosis.

Acknowledgements

Funding: None. Conflicts of interests: The authors have no relevant financial or non-financial interests to disclose.

References

1. Tomiguchi S, Tashiro K, Shiraishi S, Yoshida M, Kawanaka K, Takahashi Y, et al. Estimation of ^{123}I-IMP arterial blood activity from dynamic planar imaging of the chest using a graph plot method for the quantification of regional cerebral blood flow. Ann Nucl Med. 2010; 24:387–393.
2. Matsuda H, Tsuji S, Shuke N, Sumiya H, Tonami N, Hisada K. Noninvasive measurements of regional cerebral blood flow using technetium-99m hexamethylpropylene amine oxime. Eur J Nucl Med. 1993;20:391–401.
3. Kaminaga T, Kunimatsu N, Chikamatsu T, Furui S. Validation of CBF measurement with non-invasive microsphere method (NIMS) compared with autoradiography method (ARG). Ann Nucl Med. 2001;15:61–64.
4. Ofuji A, Mimura H, Yamashita K, Takaki A, Sone T, Ito S. Development of a simple non-invasive microsphere quantification method for cerebral blood flow using I-123-IMP. Ann Nucl Med. 2016; 30:242–249.
5. Ofuji A, Nagaoka R, Yamashita K, Takaki A, Ito S. A simple noninvasive I-123-IMP autoradiography method developed by modifying the simple noninvasive I-123-IMP microsphere method. Asia Ocean J Nucl Med Biol. 2018;6:50–56.
6. Yamashita K, Uchiyama Y, Ofuji A, Mimura H, Okumiya S, Takaki A, et al. Fully automated input function determination program for simple noninvasive I-123-IMP microsphere cerebral blood flow quantification method. Phys Med. 2016; 32:1180–1185.
7. Ito S, Takaki A, Inoue S, Tomiguchi S, Shiraishi S, Akiyama Y, et al. Improvement of the (99m) Tc-ECD brain uptake ratio (BUR) method for measurement of cerebral blood flow. Ann Nucl Med. 2012; 26:351–358.
8. Nagaoka R, Ofuji A, Yamashita K, Tomimatsu T, Orita S, Takaki A, et al. Usefulness of an automated quantitative method for measuring regional cerebral blood flow using 99mTc ethyl cysteinate dimer brain uptake ratio. Asia Ocean J Nucl Med Biol. 2015;3:77–82.
9. Masunaga S, Uchiyama Y, Ofuji A, Nagaoka R, Tomimatsu T, Iwata A, et al. Development of an automated ROI setting program for input function determination in Tc99m-ECD noninvasive cerebral blood flow quantification. Phys Med. 2014; 30:513–520.
10. Lee E, Cho B, Kwak J, Jeong C, Park MJ, Kim SW, et al. Deep learning proton beam range estimation model for quality assurance based on two-dimensional scintillated light distributions in simulations. Med Phys. 2023. doi: 10.1002/mp.16646.
11. Gaudez S, Ben Haj Slama M, Kaestner A, Upadhyay MV. 3D deep convolutional neural network segmentation model for precipitate and porosity identification in synchrotron X-ray tomograms. J Synchrotron Radiat. 2022;29:1232–1240. doi: 10.1107/S1600577522006816.
12. Liu T, Bai Y, Du M, Gao Y, Liu Y. Susceptible-infected-removed mathematical model under deep learning in hospital infection control of novel coronavirus pneumonia. J Healthc Eng. 2021;2021:1535046. doi: 10.1155/2021/1535046.
13. Hashimoto F, Ito M, Ote K, Isobe T, Okada H, Ouchi Y. Deep learning-based attenuation correction for brain PET with various radiotracers. Ann Nucl Med. 2021; 35:691–701. doi: 10.1007/s12149-021-01611-w.
14. Armanious K, Hepp T, Küstner T, Dittmann H, Nikolaou K, La Fougère C, et al. Independent attenuation correction of whole-body [18F]FDG-PET using a deep learning approach with generative adversarial networks. EJNMMI Res. 2020;10:53. doi: 10.1186/s13550-020-00644-y.
15. Yin XX, Sun L, Fu Y, Lu R, Zhang Y. U-net-Based medical image segmentation. J Healthc Eng. 2022;2022:4189781. doi: 10.1155/2022/4189781.
16. Sun H, Jiang Y, Yuan J, Wang H, Liang D, Fan W, et al. High-quality PET image synthesis from ultra-low-dose PET/MRI using bi-task deep learning. Quant Imaging Med Surg. 2022;12:5326–5342. doi: 10.21037/qims-22-116.

17. Ronneberger O, Fischer P, Brox T. U-Net: Convolutional Networks for Biomedical Image Segmentation. In: Navab, N., Hornegger, J., Wells, W., Frangi, A. (eds) Medical Image Computing and Computer-Assisted Intervention—MICCAI 2015. Cham: Springer; 2015. doi:10.1007/978-3-319-24574-4_28.
18. Rasband, W. S. ImageJ, U. S. National Institutes of Health, Bethesda, Maryland, USA (1997–2012). http://imagej.nih.gov/ij/.
19. Schneider, C. A., Rasband, W. S. & Eliceiri, K. W. NIH Image to ImageJ: 25 years of image analysis. Nat. Methods 9, 671–675 (2012). https://doi.org/10.1038/nmeth.2089.
20. Stacy EW. A generalization of the gamma distribution. Ann Math Statist. 1962;33:1187–1192. doi: 10.1214/aoms/1177704481.
21. Matsuyama Y. Hidden Markov model estimation based on alpha-EM algorithm: Discrete and continuous alpha-HMMs. The 2011 International Joint Conference on Neural Networks; 2011. pp. 808–816. doi: 10.1109/IJCNN.2011.6033304.
22. Dempster AP, Laird NM, Rubin DB. Maximum likelihood from incomplete data via the EM algorithm. J R Stat Soc B (Methodol). 1977;39:1–22. doi: 10.1111/j.2517-6161.1977.tb01600.x.
23. Do CB, Batzoglou S. What is the expectation maximization algorithm? Nat Biotechnol. 2008;26:897–899. doi: 10.1038/nbt1406.
24. Weerakoon S, Fernando TGI. A variant of Newton's method with accelerated third-order convergence. Appl Math Lett. 2000;13:87–93.
25. Kamiya Y, Ota S, Okumiya S, Yamashita K, Takaki A, Ito S. Uptake index of 123I-metaiodobenzylguanidine myocardial scintigraphy for diagnosing lewy body disease. Asia Ocean J Nucl Med Biol. 2017;5:37–43. doi: 10.22038/aojnmb.2016.7972.
26. Kamiya Y, Ota S, Tanaka Y, Yamashita K, Takaki A, Ito S. Development of an 123I-metaiodobenzylguanidine myocardial three-dimensional quantification method for the diagnosis of lewy body disease. Asia Ocean J Nucl Med Biol. 2018;6:129–138. doi: 10.22038/aojnmb.2018.10595.
27. Couette A, Tron C, Golbin L, Franck B, Houssel-Debry P, Frouget T, et al. Area under the curve of tacrolimus using microsampling devices: Towards precision medicine in solid organ transplantation? Eur J Clin Pharmacol. 2023 Sep 19. doi: 10.1007/s00228-023-03566-5.
28. Zhao C, Wang Y, Shao Y. A bioequivalence trial of dienogest in healthy Chinese participants under fed conditions. Clin Pharmacol Drug Dev. 2023 Sep 24. doi: 10.1002/cpdd.1324.
29. Moore CF, Weerts EM, Kulpa J, Schwotzer D, Dye W, Jantzi J, et al. Pharmacokinetics of oral minor cannabinoids in blood and brain. Cannabis Cannabinoid Res. 2023;8(S1):S51–S61. doi: 10.1089/can.2023.0066.